Surface Science xxx (2016) xxx–xxx

Contents lists available at ScienceDirect

Surface Science

journal homepage: www.elsevier.com/locate/susc

Elucidating the electronic structure of supported gold nanoparticles and its relevance to catalysis by means of hard X-ray photoelectron spectroscopy

Benjamin N. Reinecke [a], Kendra P. Kuhl [a], Hirohito Ogasawara [c], Lin Li [b], Johannes Voss [c], Frank Abild-Pedersen [c], Anders Nilsson [c], Thomas F. Jaramillo [a,b,c,*]

[a] Department of Chemical Engineering, Stanford University, 443 Via Ortega, Shriram Center, Stanford, CA 94305, USA
[b] SUNCAT Center for Interface Science and Catalysis, Stanford University, Stanford, CA 94305, USA
[c] SUNCAT Center for Interface Science and Catalysis, SLAC National Accelerator Laboratory, 2575 Sand Hill Road, Menlo Park, CA 94025, USA

ARTICLE INFO

Article history:
Received 28 October 2015
Received in revised form 22 December 2015
Accepted 22 December 2015
Available online xxxx

Keywords:
Gold nanoparticles
Transmission electron microscopy
Valence band
Support effect
Titanium dioxide
Hard X-ray photoelectron spectroscopy

ABSTRACT

We report on the electronic structure of Au (gold) nanoparticles supported onto TiO_2 with a goal of elucidating the most important effects that contribute to their high catalytic activity. We synthesize and characterize with high resolution transmission electron microscopy (HRTEM) 3.4, 5.3, and 9.5 nm diameter TiO_2-supported Au nanoparticles with nearly spherical shape and measure their valence band using Au 5d subshell sensitive hard X-ray photoelectron spectroscopy (HAXPES) conducted at Spring-8. Based on density functional theory (DFT) calculations of various Au surface structures, we interpret the observed changes in the Au 5d valence band structure as a function of size in terms of an increasing percentage of Au atoms at corners/edges for decreasing particle size. This work elucidates how Au coordination number impacts the electronic structure of Au nanoparticles, ultimately giving rise to their well-known catalytic activity.

1. Introduction

At this point in time it has been well-established that whereas bulk gold is catalytically inert, gold nanoparticles <10 nm diameter supported onto metal oxides can be highly catalytically active for a number of reactions, including low temperature CO oxidation [1], water gas shift (WGS) [2], and NO reduction [3], and also selective for important oxidation and hydrogenation reactions where selectivity is crucial, e.g. propene to propene oxide [4] and 1,3 butadiene to 1-butene [5], respectively. However, the origin of the nanoscaling effect on catalysis by gold (Au) is still debated [6]. The leading explanations for enhanced activity are depicted schematically in Fig. 1 and are enumerated in Table 1, a list to which we shall refer throughout this work in discussing the possible origins of catalytic activity.

In short, there are two general classifications of nanoscale effects, those that are predominantly geometric in nature and those that are electronic in nature. The predominantly geometric effects have to do with the physical orientation of Au atoms that can change with size [7,8], shape [8–11], lattice strain [11,12], and the Au-support perimeter [7]; while the predominantly electronic effects can arise from charge transfer to/from the support [13–18], or from quantum size effects [19–22].

With so many proposed explanations for the high activity of small supported gold nanoparticles, an approach is needed to experimentally disentangle these effects and assess which of these are dominant in contributing to catalytic activity; not a trivial undertaking as many of the effects are correlated with one another.

Critical to sorting out these effects is understanding the valence band electronic structure of supported Au nanoparticles. This, along with detailed knowledge of the physical structure of the nanoparticles regarding size and shape, can be particularly helpful in understanding trends in catalysis [23–26]. This approach has been applied in the field of catalysis over a wide range chemical and electrochemical reactions, e.g. the oxygen reduction reaction (ORR) in fuel cells [27] and CO oxidation in conventional heterogeneous catalysis [24].

To this end, a number of studies have measured the valence band electronic structure of Au nanoparticles supported onto TiO_2 [19,28], Al_2O_3 [29], and NiO [16] using ultraviolet photoelectron spectroscopy (UPS, ~40 eV) and Au nanoparticles supported onto carbon [30–33] using conventional Al Kα X-ray photoelectron spectroscopy (XPS, 1486 eV). UPS and conventional XPS have been valuable in understanding the electronic structure of Au nanoparticles. One key point resulting from these studies is that a metal-insulator transition occurs as a function of size, observed between Au_{55} and Au_{33}, ascribed to quantum

* Corresponding author at: Department of Chemical Engineering, Stanford University, 381 North-South Mall, Stanford, CA 94305, USA.
E-mail address: jaramilo@stanford.edu (T.F. Jaramillo).

http://dx.doi.org/10.1016/j.susc.2015.12.025
0039-6028/

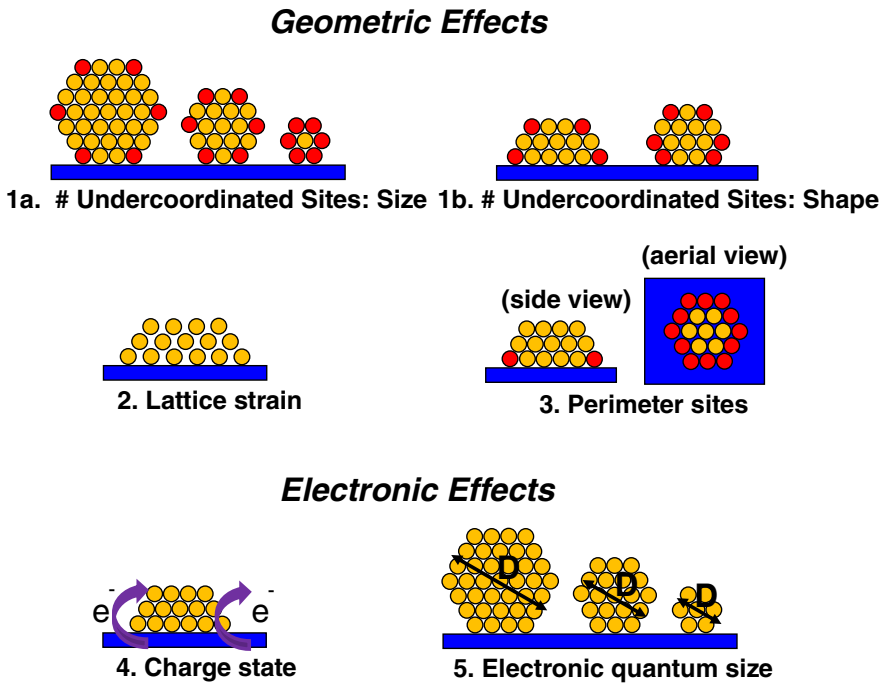

Fig. 1. Nanoscaling origins of Au catalysis. Schematic showing possible nanoscale origins of gold catalysis. Red atoms in 1a and 1b indicate undercoordinated atoms. Red atoms in 3 indicate perimeter sites.

size effects. However, UPS and conventional XPS have their limitations, as it has been found that for many supports the main spectral features of the Au d-band are generally difficult to distinguish as the nanoparticle size decreases or as gold coverage decreases, due to a heavy background valence band signal from the support that overlaps with the signal from the Au nanoparticles [16,19,28–30].

Another means to study Au d-band structure is through electronic structure theory calculations. Density functional theory (DFT) calculations have revealed that undercoordinated gold atoms have d states that are higher in energy than their corresponding full coordinated bulk gold atoms [10] and thus bind adsorbates such as O_2 more strongly. This provides a compelling explanation for the enhanced CO oxidation activity of small gold nanoparticles.

Given the importance of a catalyst's electronic structure in determining its catalytic activity, there remains a critical need to measure the valence band of gold nanoparticles in a manner uninhibited by the metal oxide support signal, and with high-energy resolution. We accomplish this by using an unconventional form of XPS, the hard X-ray (8 KeV) photoelectron spectroscopy (XPS) beam-line (BL47) at the Spring8 Synchrotron. Due to the proportionately large photoionizaiton cross-section of the Au 5d subshell versus those of the metal oxide support at this photon energy, we are able to straightforwardly deconvolute any signal from the metal oxide support in the valence band that could otherwise overwhelm the valence band signal from a submonolayer of Au nanoparticles. Our study also employs DFT calculations to help interpret the spectral features that we observe. For our studies, we chose TiO_2 as a support since it is known as one of the more active supports for Au nanoparticle catalysis and does not contribute to CO oxidation on its own [34]. In this manuscript, we aim to fill the gaps in our current knowledge within the area of Au nanoparticle catalysis by addressing the following two key questions for Au nanoparticles supported onto TiO_2: (1) How does the physical structure of the Au nanoparticles, e.g. size, shape, and lattice constant/strain, influence its valence band electronic structure? (2) How can knowledge of the electronic structure help sort out the different possible origins of catalytic activity, and help determine which are most important within our system of study?

Our approach to answering these questions is outlined here. We started by synthesizing size-controlled Au nanoparticles onto a flat, well-defined, conductive TiO_2 support by means of a ligand-free synthetic method in an effort to avoid organic contaminants. High-resolution transmission electron microscopy (HRTEM) was used to measure the size, shape, and lattice constant/strain of the supported gold nanoparticles. With detailed knowledge of these physical characteristics, we then measured the electronic structure of the Au nanoparticles by means of hard X-ray (~8 KeV) photoelectron spectroscopy (XPS). With this incident photon energy, the ratio of the absorption cross-section for the valence 5d electrons of gold to the photoionizaiton cross-section for the O 2p and Ti 3d valence electrons from the TiO_2 support is predicted (Fig. 2) to be an order of magnitude greater than with conventional Al Kα X-rays at 1486 eV (~1500 eV), and two orders of magnitude greater than with UV photons (~40 eV) [35].

Using hard X-rays allowed us to see an enhanced signal from gold versus the background TiO_2, which to the best of our knowledge has not yet been reported for catalytically relevant oxide supported gold nanoparticles. Based on our findings described below, we believe that selectively probing 5d transition metal catalysts on oxide supports could become very important to achieve the objective of

Table 1
Leading nanoscaling effects in gold catalysis.
The nanoscaling effects are broken down into geometric and electronic effects, each with selected references from the literature that support the importance of the effect.

Geometric effects		Associated references
1. Exposing catalytically active/undercoordinated gold sites by changing:	a. Size	[7,8]
	b. Shape	[8–11]
2. Lattice strain		[11,12]
3. Unique gold/support perimeter sites		[7]
Electronic effects		
4. Charge state		[13–18]
5. Quantum size		[19–22]

Please cite this article as: B.N. Reinecke, et al., Elucidating the electronic structure of supported gold nanoparticles and its relevance to catalysis by means of hard X-ray photoel..., Surf. Sci. (2016), http://dx.doi.org/10.1016/j.susc.2015.12.025

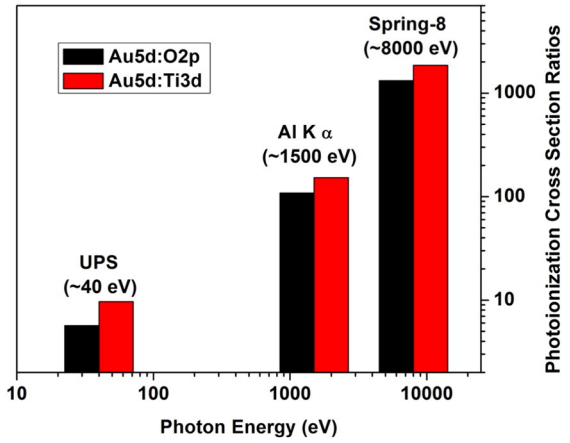

Fig. 2. Photoionization cross-section ratios. Theoretical calculation of the Au 5d/O 2p and Au 5d/Ti 3d photoelectron cross-section ratios at three different photon energies (~40 eV, ~1500 eV, and ~8 KeV) [35].

correlating valence band structure to catalytic performance in many areas of catalysis.

2. Experimental

2.1. Sample preparation

First, 1400 Å of titanium was deposited by electron beam evaporation onto silicon(111) (0.001 ohm * cm) in a clean room environment using an Innotec ES26C evaporation system. The rate of deposition was 0.15 Å/s for 5 min and then ramped to 2 Å/s for the remainder of the deposition. The chamber temperature and pressure were 45 °C and 2×10^{-7} torr, respectively. The titanium film was then exposed to ambient air to form a thin TiO_2 native oxide. Finally, 3, 8, and 20 Å nominal thicknesses of gold were electron beam deposited at a rate of 0.15 Å/s onto several titanium-metalized Si wafers to achieve three different sized gold nanoparticles on TiO_2, respectively. The chamber temperature and pressure were 30 °C and 2×10^{-7} torr during Au deposition. The remaining gold-free, titanium metalized Si wafers provided background controls for electronic structure measurements. The bulk gold surface studied in this investigation consisted of an evaporated film of gold on a copper substrate that is stored inside the ultra-high vacuum chamber at beam-line 47XU at the Spring8 Synchrotron. That sample will be referred to as "bulk gold" from this point on.

2.2. Transmission electron microscopy (TEM)

The supported gold nanoparticles were examined in an FEI Tecnai G2 F20 X-Twin Transmission Electron Microscope (TEM) to determine the size distribution and shape. Both plan view (top–down) and cross sectional view (side-on) samples are prepared using standard TEM preparations which included: heating of the sample with crystal bond to 180 °C for use as a binder, SiC film lapping, diamond film lapping, alumina slurry dimpling, and Ga ion milling.

2.3. Electronic structure measurements

The valence band and the Au 4f X-ray photoelectron spectra for the TiO_2 bare support, the three different TiO_2 supported gold nanoparticle samples, and bulk gold were measured at the Spring-8 Synchrotron, BeamlineBL47XU, and the hard X-ray photoelectron spectroscopy (HAXPES) beam-line, at a photon energy of 7945 eV (~8 KeV). Photoelectrons were collected using a GammadataScienta R4000 spectrometer with a total resolution better than 0.25 eV. Each photoelectron spectrum was measured by illuminating the x-ray beam at 1° incidence to the surface and collecting the appropriate photoelectrons at 89° to the surface plane. Additionally, the Ti 2p region was collected for analysis of the TiO_2 support and to rule out any charging induced binding energy shifts or broadening among the XPS spectra of the gold nanoparticles.

2.4. Electronic structure calculations

The electronic structures of Au surfaces with various coordination numbers were determined from density functional theory (DFT) calculations using the Quantum Espresso code [36]. The (100), (111), and (211) surfaces were modeled using $2 \times 2 \times 6$ slabs, with 20 Å of vacuum. The (421) surface was modeled using a 36 atom (1×1) surface unit cell, containing five close-packed layers, with 13 Å of vacuum. The Crystallographic Information File (CIF) of each model is provided as supporting information: Au100.cif, Au111.cif, Au211.cif, Au421.cif, and Aubulk.cif. For all surfaces, Brillouin zone sampling with a grid-spacing of no more than 0.05 $Å^{-1}$ with Fermi smearing of $k_BT = 0.1$ eV was used, and the Kohn–Sham bands were expanded in plane wave basis sets with 500 eV cut off. Static calculations were carried out using the experimental lattice constant, 4.08 Å [34], and for 3% compressive strain (in all X–Y–Z). Generalized gradient approximation (PBE [35,36]) was used to describe the exchange–correlation effects. Spin–orbit coupling was taken into account by using an ultrasoft pseudopotential with *j*-dependent projectors [37,38]

3. Results & discussion

3.1. Physical characterization

Electron beam evaporation produces size-controlled gold nanoparticles with a very high surface density, as depicted in the TEM images in Fig. 3. Both low magnification and high-resolution (HR-TEM) images of the three samples in plain view are shown in Fig. 3 (1-A, 1-C, and 1-E) and (2-A, 2-C, and 2-E), respectively. The particles are mostly circular in cross-section, with the following average diameters: 3.4 nm, 5.3 nm, and 9.5 nm with an error in the mean of 0.1 nm, 0.1 nm, and 0.2 nm, respectively. These results agree well with SEM observations (see supporting information).

By imaging the samples in cross-section, we are able to directly observe the nature of the TiO_2 support and the shape of the gold nanoparticles, shown in Fig. 3 (1-B, 1-D, and 1-F and 2-B, 2-D, and 2-F). The native TiO_2 layer (see supporting information) can be seen clearly by the contrast between the polycrystalline titanium phase and the TiO_2 layer on top from Fig. 3 (1-F). The thickness of the TiO_2 layer is roughly 6 nm, indicated by a pair of arrows. The thickness as measured by XPS (see supporting information) is 1.1 nm. The difference between the XPS and TEM derived thickness measurements is most likely due to the 180 °C heating step during TEM preparation, which likely causes growth in the TiO_2 layer. The cross-sectional TEM images show that the gold nanoparticles bind to the TiO_2 surface in a spherical but slightly flattened form (see supporting information). We have ruled out significant shape change or sintering of the gold nanoparticles during TEM preparation or imaging based on comparisons of size and surface density (# particles/area) in SEM versus TEM (see supporting information).

Since the particles are nearly spherical, the diameters as determined from the TEM plan view are used throughout the discussion. The histograms of each nanoparticle size and associated standard deviation as determined by TEM plan view imaging are shown in the insets of Fig. 3 (1-A, 1-C, and 1-E). It has been shown previously that the truncated octahedron geometry fits well for small nanoparticles of face centered cubic (FCC) metals such as gold [39] and has been used to model supported gold catalysts [10]. As such, it is assumed that each nearly spherical gold nanoparticle is a truncated octahedron of the closest size to that which we measure by TEM. The model is shown in Fig. 4.

Please cite this article as: B.N. Reinecke, et al., Elucidating the electronic structure of supported gold nanoparticles and its relevance to catalysis by means of hard X-ray photoel..., Surf. Sci. (2016), http://dx.doi.org/10.1016/j.susc.2015.12.025

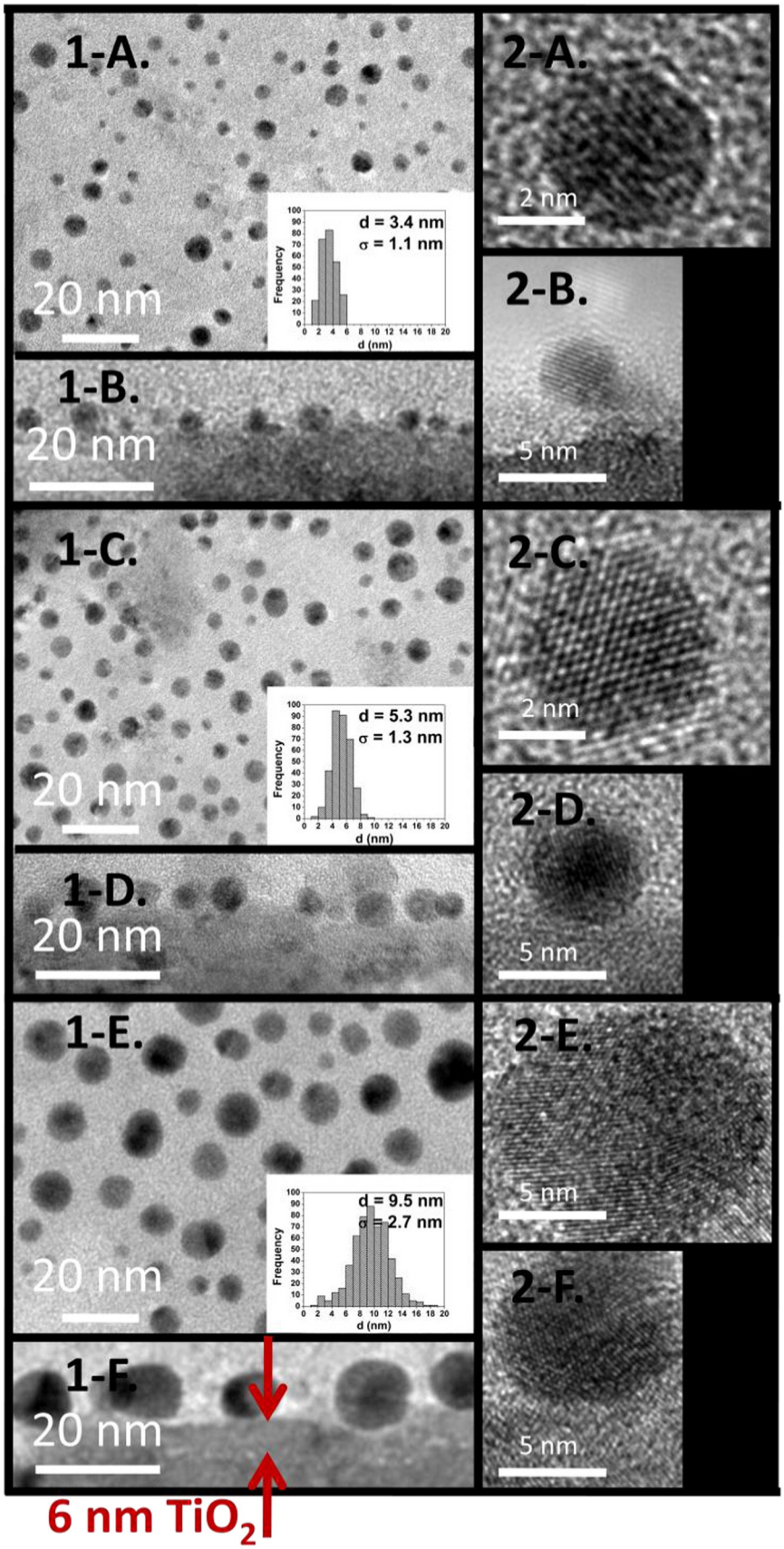

Fig. 3. Au nanoparticle imaging. Morphology, size, size distribution, and atomic scale features of gold nanoparticles on TiO2 as observed by TEM. The gold nanoparticles of 3 Å, 8 Å, and 20 Å nominal deposition thickness are shown in the top row, middle row and bottom row, respectively. The TEM low resolution and high resolution images of the gold nanoparticles are shown in 1-A through 1-F and 2-A through 2-F, respectively, with the top-down (plan) views noted A, C, and E and with the cross-sectional views noted B, D, and F. Additionally, the histograms for the TEM plan-view based nanoparticle diameter distributions are shown as insets to 1-A, 1-C, and 1-E. Finally, a TiO2 layer thickness of around 6 nm is indicated on 1-F with arrows that define the boundaries of the oxide layer above the titanium metal.

Please cite this article as: B.N. Reinecke, et al., Elucidating the electronic structure of supported gold nanoparticles and its relevance to catalysis by means of hard X-ray photoel..., Surf. Sci. (2016), http://dx.doi.org/10.1016/j.susc.2015.12.025

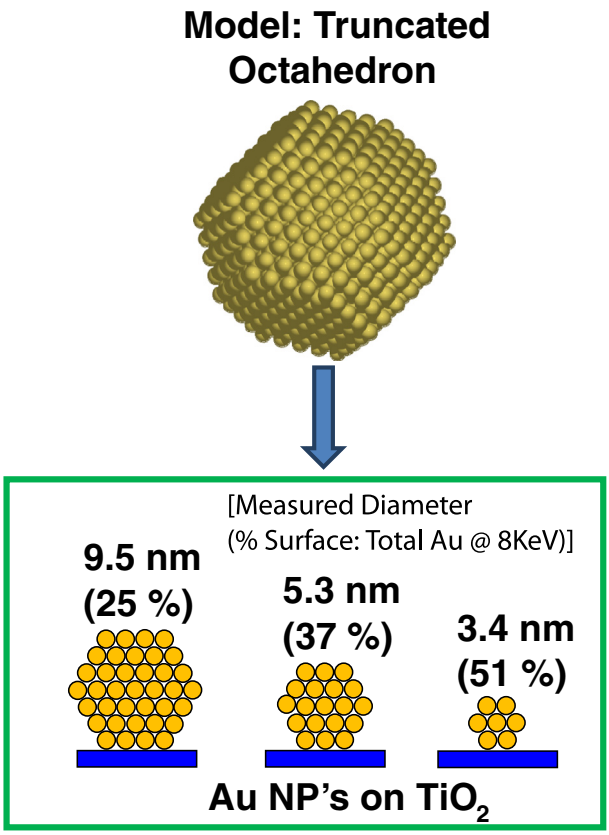

Fig. 4. Truncated octahedron model. Truncated octahedron model of a nanoparticle with associated 2D cartoon renderings of the nanoparticles of each size (3.4 nm, 5.3 nm, 9.5 nm diameter).

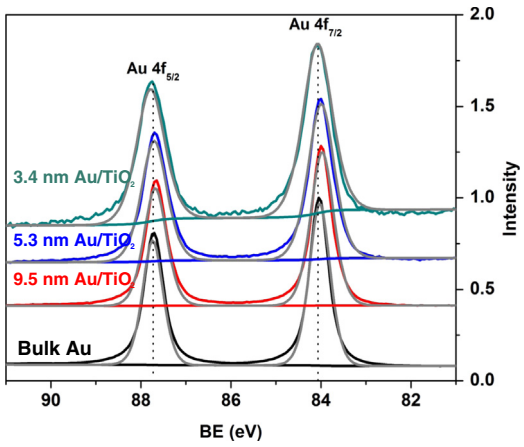

Fig. 5. Au 4f XPS. Au 4f core level spectra collected using ~8 KeV hard X-rays for each of the 3.4 nm, 5.3 nm, and 9.5 nm average diameter TiO_2-supported gold nanoparticles as well as bulk gold. Intensities have been normalized.

Shape change with size due to the support (nanoscaling effect #1b, Table 1) is therefore not an important consideration for these gold nanoparticles.

3.2. Electronic structure characterization

3.2.1. Au 4f XPS

Core-level shifts in the Au 4f spectral region have previously been used to describe changes in the chemical state [40–43] or geometric arrangement [41,44,45] of the Au surface. For all of our samples, including bulk gold and the three TiO_2-supported gold nanoparticle samples, the Au 4f core level measurements from Fig. 5 show only one doublet with the Au $4f_{7/2}$ binding energy at 84.0 ± 0.1 eV.

This agrees well with measurements on bulk metallic gold, with an Au $4f_{7/2}$ binding energy also at 84.0 eV [46], supporting the notion that all the Au nanoparticle samples are in a charge-neutral, bulk-like state. Metallic (charge-neutral) gold has been shown to be the catalytically active state for CO oxidation [47]. It should be noted that some supported gold nanoparticles in this size regime, synthesized by other methods, have been reported as having a shell of oxidation [40]. In our case there is no observable oxidation at the surface, as this would manifest itself as additional Au $4f_{7/2}$ and Au $4f_{5/2}$ contributions upshifted significantly in binding energy. Others have shown that there are a number of possible final and initial state effects that can shift the binding energy either up or down [41]. Final state (screening) effects are expected to be minute at this size regime [48], especially on a conductive support [41].

From the initial (electronic) state viewpoint, it has been found that oxygen defect sites on the TiO_2 support can anchor nanoparticles to the surface while polarizing the gold atoms bound to those anchor sites. Given the size and shape of the nanoparticles in the present study, however, the fraction of gold atoms affected in this manner is expected to be miniscule [15] and any binding energy shift due to these atoms would likely be outside of the detection capability of XPS. For example, only 3–4 atoms of Au would be affected for a 3 nm spherical gold nanoparticle on TiO_2 [15]. Given the size range studied here (3.4 nm, 5.3 nm, and 9.5 nm), electronic promotion effects are expected to be negligible as such effects have previously been found to be insignificant for gold nanoparticles above 2–3 nm in diameter on a number of oxide supports [17]. While a surface core level shift of 0.4 eV has been observed before for a gold surface [44], in our case we do not observe such an effect. To explore whether increased core level line broadening due to the heterogeneity of surface sites for a given nanoparticle size and the finite size distribution of nanoparticles could potentially mask such subtle shifts [41], we carefully examined line broadening in our samples. We observed line broadening for the smaller Au nanoparticles by virtue of an increasing full width at half max (FWHM) with decreasing nanoparticle size: The FWHM of the Au $4f_{7/2}$ peak was measured as 0.54 eV, 0.60 eV, 0.68 eV, and 0.77 eV for bulk gold, while 9.5 nm, 5.3 nm, and 3.4 nm for gold nanoparticles, respectively. Though this line broadening is measurable and indicates an increasingly heterogeneous surface with smaller nanoparticle sizes, the broadening is not sufficiently large as to mask significant (e.g. 0.4 eV) shifts in the core-level electronic structure of the Au nanoparticles. Therefore, our spectral analysis of the Au 4f core level region suggests that nanoscaling effect #4(Table 1) does not play a significant role, as the bulk gold and the 3.4 nm, 5.3 nm, and 9.5 nm in diameter gold nanoparticles are all in a charge-neutral, bulk-like state.

3.2.2. Valence band XPS

The normalized raw valence region spectra for the TiO_2 support and the 3.4 nm, 5.3 nm, and 9.5 nm gold on TiO_2 are shown in Fig. 6.

As expected from Fig. 2, there is a very large enhancement of the gold signal in the valence region as compared to the bare TiO_2 support. This enhancement increases with the amount of gold deposited. The valence region photoemission spectra after background TiO_2 subtraction of the 3.4 nm, 5.3 nm, and 9.5 nm diameter TiO_2-supported gold nanoparticles as well as that of bulk gold are shown together in Fig. 7.

The scheme used to reference the binding energy scale and procedures relating to the normalization and subtraction for all samples are described in the supporting information.

The main features of the gold valence band are evident in all four spectra. There is a broad and flat band related to d states rehybridized with s/p states [49] which extends from the Fermi level through the sharper and more intense part of the d-band that spans from roughly 2 eV to 9 eV. Although there is a slight shift observed at

Please cite this article as: B.N. Reinecke, et al., Elucidating the electronic structure of supported gold nanoparticles and its relevance to catalysis by means of hard X-ray photoel..., Surf. Sci. (2016), http://dx.doi.org/10.1016/j.susc.2015.12.025

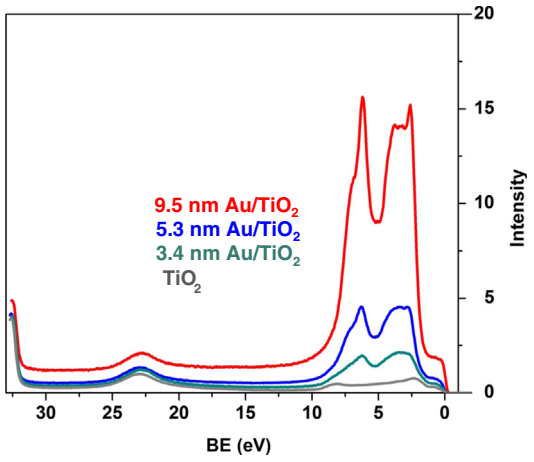

Fig. 6. Total valence band X-ray photoelectron spectroscopy. Total valence band photoelectron spectra collected using ~8 KeV hard X-rays for blank TiO_2 (gray), 3.4 nm (dark cyan), 5.3 nm (blue), and 9.5 nm (red) gold nanoparticles on TiO_2 normalized with the Ti 3p (0) peak area at BE = ~32.5 eV.

the Fermi edge for the 3.4 nm Au nanoparticles, this is within the estimated experimental resolution (~0.25 eV) and is within reasonable error due to the method of TiO_2 background subtraction (see supporting information). The observation of occupied states at the Fermi Level implies that the gold is metallic, therefore there is no observed quantum size effect (nanoscaling effect #5, Table 1) within this size regime (3.4–9.5 nm).

The sharper and more intense part of the d-band shows a number of peaks, as is expected for the bulk gold valence band spectrum [50,51]. To facilitate comparisons among all samples, we will focus our attention on features observed in the vicinity of 3.5 eV. For bulk gold, this feature consists of a trough surrounded by two clear peaks. The data shows a clear trend with particle size regarding this feature; the trough gradually fills in as the gold nanoparticle size decreases, until, at the smallest size (3.4 nm), there is only one broad peak around 3.5 eV. While there are other, more subtle changes in the valence band spectra, this particular difference among the samples is the most prominent.

Morphology and support can play significant roles in the electronic structure of Au nanoparticles. Previously, it was found for thin Au nanoparticles several monolayers thick on Al_2O_3 [29] and NiO [16] and Au mono/bi/multilayers on TiO_x [19] that the lower binding energy peak of the Au d-band shifts to higher binding energies. We do not observe this shift, which suggests that such a shift may be related to an intimate

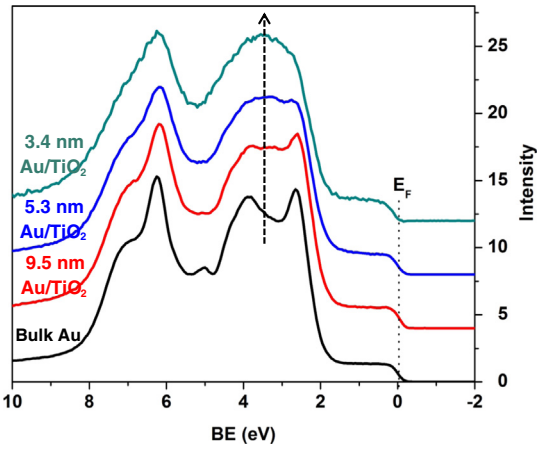

Fig. 7. Au valence band. Valence band spectrum of the Au d-band after TiO_2 background subtraction for 3.4 nm, 5.3 nm, and 9.5 nm diameter gold nanoparticles on TiO_2. Bulk gold is shown for reference.

contact with the support since our nanoparticles are spherical and are not intimately contacting the TiO_2. In support of this hypothesis is other work on spherical gold nanoparticles 1.6–10 nm in diameter on a "non-interacting" carbon support, which found that the two main d-band features remain essentially the same [30]. We thus attribute the filling in of the trough in the d states observed at ~3.5 eV to an intrinsic gold nanoparticle effect, not a support effect, which synchrotron radiation enables us to observe more clearly within the valence band region than observed by others using more conventional methods.

3.2.2.1. Valence band hypothesis, nanoscaling effects #1a and/or #2 (Table 1)?. It has been suggested previously that undercoordinated Au atoms at the nanoparticle surface with coordination numbers (CN) 6 & 7 are the most active sites for the CO oxidation reaction [10]. Undercoordinated sites at the surface can facilitate the reaction's rate determining step and activate molecular O_2 [52] because these undercoordinated atoms relative to bulk atoms have markedly higher energy d-states, which leads to stronger adsorbate interactions [10]. As the nanoparticle size decreases, the ratio of surface atoms and especially undercoordinated surface atoms to bulk atoms increases, which could, at least in part, explain the observed filling in of the d-band of Au with decrease in size.

Straining lattice parameter is also expected to have an effect on both its catalytic activity as well as its d-band structure [53], and therefore could, at least in part, explain the changes we observe in the d-band of our supported Au nanoparticles. In light of this, we attempted to address lattice-straining effects by measuring the d spacing of a variety of differently sized Au nanoparticles in HRTEM. The variability in the derived Au–Au bond length using this method, in some cases greater than 3%, precludes us from making any conclusive statements regarding the potential straining of the lattice. Nevertheless, previous EXAFS studies have shown that the overall compressive strain in Au nanoparticles above ~3 nm in diameter is at most ~1%, with the compressive strain becoming more prominent below this size [54–56]. This implies that for the size regime explored in our study (3.4, 5.3, and 9.5 nm diameter) the overall strain in the nanoparticle should not be a major factor. Surface and near surface straining, however, plays a critical role in gold nanoparticles 3–5 nm in diameter, as determined by diffraction experiments [57] and therefore must be considered as a possible cause of the observed changes in electronic structure.

Therefore, our spectroscopic measurements of the Au valence band (Fig. 7) suggest that the filling in of the trough in the d states with decreasing nanoparticle size can be attributed to an increase in the proportion of surface gold atoms probed by the XPS experiment that contains an increasing proportion of undercoordinated Au atoms (e.g. CN 6 and 7) and/or that exhibit surface (near surface) strain.

Our approach to test the coordination number and/or surface straining hypothesis is to computationally generate the gold d-band for each of the 3.4 nm, 5.3 nm, 9.5 nm nanoparticles and bulk gold considering the effects of both coordination number and strain and then compare with the experimental XPS results. To realize this, we consider that each gold atom within the truncated octahedron model (Fig. 4) has its d-band fully specified by CN and either no strain or a reasonable degree of contractile strain (3%). For these calculations, we use periodic DFT and obtain d-band spectra of gold atom coordination numbers of 6, 7, 8, 9 and 12 using model periodic surfaces of Au(111), Au(100), Au(110), Au(211), and Au(421) slabs (see supporting information) that are either unstrained or contractile strained in all X–Y–Z by 3%.

Shown in Fig. 8 is an example of the d-band for a gold CN 7 atom (step edge) from a Au (211) slab that is not strained, one that is strained, and a gold CN 12 atom from a bulk Au crystal that is not strained.

The d-band for gold atoms with CN 7 is markedly shifted toward the Fermi level compared to the d-band of CN 12 atoms, with some broadening of the d-band due to the effects of strain. Interestingly, the d-band of CN 7 atoms (strained or unstrained) peaks at approximately the same region where, in our d-band measurements of supported Au

Please cite this article as: B.N. Reinecke, et al., Elucidating the electronic structure of supported gold nanoparticles and its relevance to catalysis by means of hard X-ray photoel..., Surf. Sci. (2016), http://dx.doi.org/10.1016/j.susc.2015.12.025

nanoparticles, we observe the filling in of the trough. This lends credence to the hypothesis that the surface coordination number and/or surface (or near surface) straining can explain the systematic changes in the d-band measurements at approximately 3.5 eV (Fig. 7).

The d-DOS of each coordination number Au atom (strained or unstrained) is then inputted into the truncated octahedron geometric model (or a simple flat surface model for the bulk Au), taking into account effects such as XPS attenuation through the Au atoms, finite nanoparticle size distribution, and the expected geometrical statistics of Au atoms with various coordination numbers within the truncated octahedron model of each relevant sizes. In total, this model appropriately captures some of the most important experimental features that are expected to be present within the measured spectra so that a one to one comparison can be made between the measured and the calculated spectra. The full model is described in detail in the supporting information.

Fig. 9 A–C shows the calculated d-DOS for the three nanoparticle sizes and bulk Au for the cases where all Au atoms are strained (3% contraction) (Fig. 9A), only the top layer Au atoms are strained (3% contraction) (Fig. 9B), and where none of the Au atoms are strained (Fig. 9C), and compares these cases to the measurement (Fig. 9D).

The important observation from this comparison is that there is a filling in effect in the ~3.5 eV region for all calculated d-bands (Fig. 9A–C) with a decrease in nanoparticle size. This effect is present regardless of whether all atoms are strained, only top layer atoms are strained, or no atoms are strained, which strongly suggests that the observed filling in of the d-band trough around 3.5 eV in the measured spectra (Fig. 9D) is primarily due to coordination number effects only and less so to surface (or near surface) strain. While surface (or near surface) strain is still likely present and could potentially still have an impact on the catalytic activity, it apparently has little effect on the d-band structure of Au within our system.

The other differences that are observed in regions outside of where the d-band trough is present (~3.5 eV) should be mentioned briefly, keeping in mind their peripheral nature to our main conclusion. 1. A small shift in relative binding energies of the d-band structure comparing Fig. 9A–C to D, which indicates that the theoretical method is appropriately capturing the d-band of Au, but is not perfect, given the well-known relativistic effects in Au [34]. 2. An obvious broadening of the entire d-band upon compressing the entire lattice by 3% (Fig. 3A vs. C), which is expected for transition metals with d electron counts 5–10 [53]. 3. The discrepancy in the trend in the d-band intensities at > ~5.5 eV compared between any of the calculated and the measured cases, which does not yet have an explanation. 4. There is a discrepancy in the intensities in the 0–2 eV region between any of the calculated and measured d-bands. This region is well known to exhibit the low binding energy component of the relatively flat sp–d re-hybridization states in

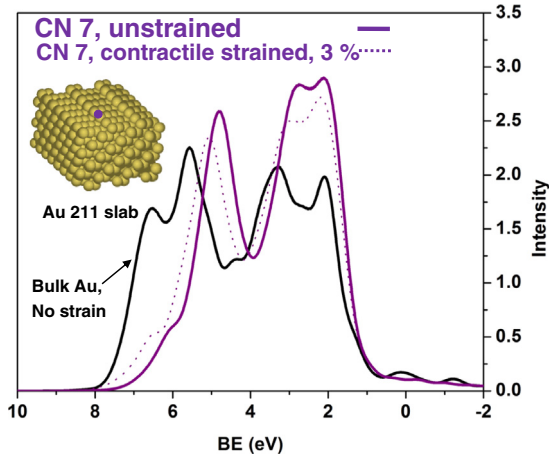

Fig. 8. Calculated Au step edge atom d-band. The calculated d-band of the step edge atoms (CN 7) with or without strain is significantly different from that of bulk, unstrained atoms (CN 12). 3% contractile strain on CN 7 atoms resulted in a slight broadening. Inset: A Au(211) slab with CN 7 step edge atom.

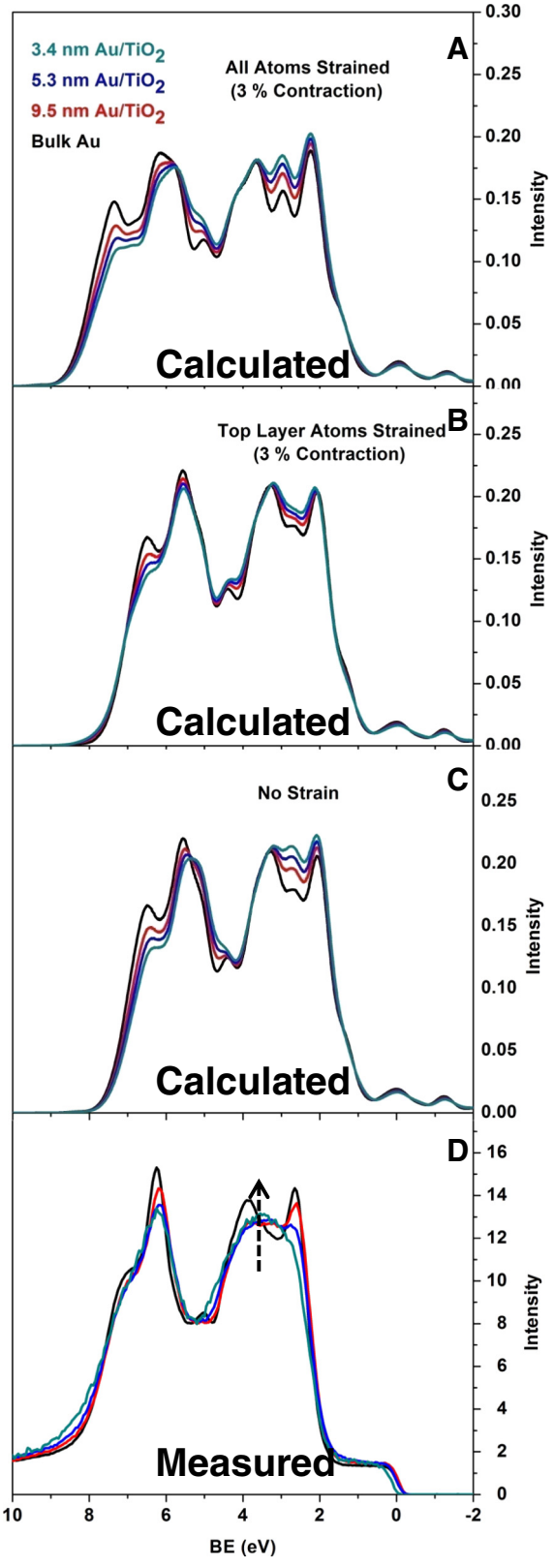

Fig. 9. Au/TiO_2 electronic structure: calculated vs. measured Au d-band. The top three graphs show the effects of 3% contractile strain on all atoms (A), top layer atoms only (B), and none of the atoms (C). The bottom graph is the measured spectra at 8 KeV (D).

the measured spectra [30,49] and may be difficult to capture by our methods of calculation.

Therefore, the filling in that we observe in the d-band trough of gold nanoparticles with decrease in size is primarily due to an increased percentage of surface Au atoms, an increasing proportion of which are undercoordinated (CN 6 and 7).

Generally speaking, the observed changes in the trough region (~3.5 eV) of the d-band as a function of size should be present regardless of the support material, however different support materials could still potentially influence the Au electronic structure through other means, e.g. if the support directs the shape of the gold nanoparticle to expose more or fewer of the low CN gold sites. These low CN sites (steps [CN 7] and corners [CN 6]) are thought by some to be the active sites in gas phase CO oxidation catalysis [8,58]. Therefore, the filling in of the trough in the gold d-band with decreasing nanoparticle size can be attributed to nanoscaling effect # 1a (Table 1), which helps explain the known catalytic activity of Au at the nanoscale. This effect is categorized as a geometric effect where the local geometric structure of the atoms ultimately dictates electronic structure.

3.2.2.2. Valence band hypothesis, considering other effects. While the CN of atoms at the gold surface can at least partially explain the experimentally observed filling in of the d-band trough, we have also considered a number of alternative possibilities: gold at the interface with TiO_2, including unique perimeter sites; amorphization; gold atoms at the surface to which molecules (C, N_2, O_2) are adsorbed; and re-hybridization of the d states with s or p states with size.

Regarding interfacial or perimeter sites in contact with the TiO_2, the only way that these sites could give rise to such marked changes in the measured XPS spectra is if the shape of the gold nanoparticles yielded a large fraction of such sites; this, however, is not the case for the nanoparticles studied herein as they possess a spherical geometry with less than 1% of the atoms representing electronically perturbed interfacial or perimeter sites [15]. Even a hemispherical geometry would lead to small fractions of interfacial or perimeter sites (see calculations in the supporting information). Therefore, perimeter and interface sites can be ruled out as the cause for the experimentally observed filling in of the d-band trough. We cannot, however, rule out the possibility that perimeter sites are the active sites for catalysis (nanoscaling effect #3, Table 1); such a determination is outside the scope of the present manuscript.

We have assumed that the small gold nanoparticles can be modeled as crystalline truncated octahedron or other suitable crystalline polyhedra, however, at these small nanoparticle sizes, amorphization and disorder could play a very large role. Indeed, it was found that gold nanoparticles of 1.6 nm in diameter exhibit substantial atomic disorder [59] when immersed in solvent. However, when studied in the dry state, without solvent, much of the disordering is absent. Therefore, given that the nanoparticles in our study are much larger than those in the aforementioned literature reference and that we are studying "dry" nanoparticles, our nanoparticles should resemble more a crystalline state than a disordered, glass-like state. The TEM images shown in Fig. 3 are consistent with this view.

We have also considered the effect of small molecules adsorbed (e.g. H_2O, O_2, NO, CH_3OH) and how they might fill in of the trough in the d-band; we have ruled out this possibility as well. Most of the common adsorbates, even for Au(110) surfaces (CN 7), desorb from the gold surface considerably below room temperature [52] and especially at low pressure. The only gold surface sites that might be considered as reactive to these adsorbates are corner sites (CN 6), which comprise a much smaller proportion of the total gold atoms within the gold nanoparticles than the magnitude of the proportional change observed within the d-band (see supporting information). The same logic applies to the possible influence of sp–d re-hybridization as a function of gold nanoparticle size. The estimated perturbation of the d electron count due to sp–d re-hybridization per Au atom over the full range of sizes measured is 0.3% (see supporting information) [49], outside the detection capability of XPS. We can thus rule out sp–d re-hybridization playing a major role in affecting electronic structure changes as a function of gold nanoparticle size within the range studied here.

We thus find that the DFT calculations for different CN Au atoms with and without 3% compressive strain, combined with a straightforward geometric model of an Au nanoparticle, can explain the observed sized dependent changes in the d-band. Ultimately, the presence of surface Au atoms, an increasing proportion of which are undercoordinated (CN 6 and 7) with decreasing nanoparticle size, is responsible for the filling in of the d-band trough we observe experimentally. As undercoordinated (CN 6 and 7) atoms are thought to be the catalytically active sites on small supported gold nanoparticles, this work reveals a link between the catalytically active sites on Au nanoparticles and their electronic structure, probed by both experiment and DFT.

While the focus of this study is on nearly spherical gold nanoparticles of 3.4, 5.3, and 9.5 nm diameter deposited onto TiO_2, our approach is broadly applicable to a host of other sizes, shapes and supports. The principal advantage of our approach is the use of hard X-ray, synchrotron based XPS measurements that can discriminate small changes in the valence band features of gold, as portrayed within the region around 3.5 eV, without major contributions from the underlying metal oxide support. Measuring the valence band contributions of gold versus a 3d/4d metal oxide support at 8 KeV versus conventional Al Kα (1486 eV) XPS or standard UPS (~40 eV) amplifies the gold 5d-band cross-section relative to the valence band contributions (metal 3d/4d and O 2p) of its support by roughly one and two orders of magnitude, respectively (see supporting information). With conventional XPS or UPS, the valence band signal from the 3d/4d metal oxides would typically overwhelm that of the 5d transition metal. This benefit of using synchrotron-based hard X-rays can be applied toward the study of any 5d transition metal catalyst in which one aims to distinguish its valence band signal from 3d/4d metals or metal oxides present in the system, e.g. a 5d metal supported onto a 3d/4d metal oxide support or a metal alloy between a 5d metal and a 3d/4d metal, as has been shown in a previous study of Pt versus Cu within a Pt–Cu alloy catalyst [60].

4. Conclusions

In this work we have studied how the size and shape of gold nanoparticles supported onto TiO_2 dictate their electronic structure and how we can use the measured electronic structure to identify the origins of the well-known nanoscaling effects in gold catalysis. With these goals in mind, we synthesized and investigated ligand-free gold nanoparticles 3.4, 5.3 and 9.5 nm in diameter supported onto a flat, well-defined, thin-film TiO_2 support. High-resolution TEM imaging revealed that the nanoparticles were sitting nearly spherically on the TiO_2 support. All three investigated sizes of Au nanoparticles as well as bulk gold were found to be in a bulk-like metallic state, as determined by the Au 4f doublet from XPS. Valence band measurements using hard X-ray XPS afforded clearly distinguishable signals for Au valence band versus that from the TiO_2 support. We observe significant changes in the Au valence band as a function of Au particle size. More specifically, we measured a significant increase in intensity at a binding energy of 3.5 eV, a region between two valence band peaks in bulk Au, as a function of decreasing Au particle size. DFT calculations suggest that this is due to the proportional increase in surface Au atoms, an increasing percentage of which are undercoordinated (CN 6 and 7), with a decrease in gold nanoparticle size (nanoscaling effect #1a, Table 1). This effect of coordination number on d-band will likely occur irrespective of the choice of support, though different supports will likely still have some impact on the electronic structure of gold, e.g. through shape effects which will influence the fraction of low CN sites. By having measured discrete changes in the gold valence band structure of supported gold nanoparticles using synchrotron-based hard X-rays and utilizing

Please cite this article as: B.N. Reinecke, et al., Elucidating the electronic structure of supported gold nanoparticles and its relevance to catalysis by means of hard X-ray photoel..., Surf. Sci. (2016), http://dx.doi.org/10.1016/j.susc.2015.12.025

theoretical modeling, we have elucidated how coordination number plays a crucial role in affecting the electronic properties of nanoparticulate gold, which ultimately determines its catalytic activity. The approach utilized herein is of particular value in assessing the electronic structure of catalytically active surface sites of 5d transition metal nanoparticles supported onto standard 3d/4d metal oxide supports.

Acknowledgments

This material is based upon work supported by the National Science Foundation under Grant No. 1066515. Seed funding was provided by a Hellman Faculty Scholar Award. B.N.R. thanks the National Defense Science and Engineering Graduate (NDSEG) fellowship and the Stanford Graduate Fellowship (SGF) for fellowship support. T.F.J., H.O., L.L., J.V., F.A-P, and A.N. acknowledge support from the DOE Office of Basic Energy Science to the SUNCAT Center for Interface Science and Catalysis. This work was performed in part at the Stanford Nanofabrication Facility which is supported by National Science Foundation through the NNIN under Grant ECS-9731293.The synchrotron radiation experiments were performed at the BL47XU of SPring-8 with the approval of the Japan Synchrotron Radiation Research Institute (JASRI) (Proposal No. 2009B1751). The authors thank Eiji Ikenaga for technical assistance at the Spring8 Synchrotron. B.N.R. thanks Ann Marshall for TEM preparation training. The authors would also like to acknowledge Zhebo Chen, Arnold Forman, and Jens K. Nørskov for helpful discussions.

Appendix A. Supplementary data

Supplementary data to this article can be found online at http://dx.doi.org/10.1016/j.susc.2015.12.025.

References

[1] M. Haruta, N. Yamada, T. Kobayashi, S. Iijima, Gold catalysts prepared by coprecipitation for low-temperature oxidation of hydrogen and of carbon-monoxide, J. Catal. 115 (1989) 301.
[2] D. Andreeva, V. Idakiev, T. Tabakova, A. Andreev, R. Giovanoli, Low-temperature water–gas shift reaction on Au/alpha-Fe2O3 catalyst, Appl. Catal. A Gen. 134 (1996) 275.
[3] A. Ueda, M. Haruta, Nitric oxide reduction with hydrogen, carbon monoxide, and hydrocarbons over gold catalysts, Gold Bull. 32 (1999) (3-+).
[4] T. Hayashi, K. Tanaka, M. Haruta, Selective vapor-phase epoxidation of propylene over Au/TiO2 catalysts in the presence of oxygen and hydrogen, J. Catal. 178 (1998) 566.
[5] G.C. Bond, P.A. Sermon, G. Webb, D.A. Buchanan, P.B. Wells, Hydrogenation over supported gold catalysts, J. Chem. Soc. Chem. Commun. (1973) 444.
[6] J.L. Gong, Structure and surface chemistry of gold-based model catalysts, Chem. Rev. 112 (2012) 2987.
[7] M. Haruta, S. Tsubota, T. Kobayashi, H. Kageyama, M.J. Genet, B. Delmon, Low-temperature oxidation of CO over gold supported on TiO_2, alpha-Fe_2O_3, and CO_3O_4, J. Catal. 144 (1993) 175.
[8] T.V.W. Janssens, A. Carlsson, A. Puig-Molina, B.S. Clausen, Relation between nanoscale Au particle structure and activity for CO oxidation on supported gold catalysts, J. Catal. 240 (2006) 108.
[9] A. Carlsson, A. Puig-Molina, T.V.W. Janssens, New method for analysis of nanoparticle geometry in supported fee metal catalysts with scanning transmission electron microscopy, J. Phys. Chem. B 110 (2006) 5286.
[10] T.V.W. Janssens, B.S. Clausen, B. Hvolbaek, H. Falsig, C.H. Christensen, T. Bligaard, J.K. Norskov, Insights into the reactivity of supported Au nanoparticles: combining theory and experiments, Top. Catal. 44 (2007) 15.
[11] Y. Xu, M. Mavrikakis, Adsorption and dissociation of O2 on gold surfaces: effect of steps and strain, J. Phys. Chem. B 107 (2003) 9298.
[12] M. Mavrikakis, P. Stoltze, J.K. Norskov, Making gold less noble, Catal. Lett. 64 (2000) 101.
[13] M.A. Brown, F. Ringleb, Y. Fujimori, M. Sterrer, H.-J. Freund, G. Preda, G. Pacchioni, Initial formation of positively charged gold on MgO(001) thin films: identification by experiment and structural assignment by theory, J. Phys. Chem. C 115 (2011) 10114.
[14] E. Florez, L. Feria, F. Vines, J.A. Rodriguez, F. Illas, Effect of the support on the electronic structure of Au nanoparticles supported on transition metal carbides: choice of the best substrate for Au activation, J. Phys. Chem. C 113 (2009) 19994.
[15] N. Lopez, J.K. Norskov, T.V.W. Janssens, A. Carlsson, A. Puig-Molina, B.S. Clausen, J.D. Grunwaldt, The adhesion and shape of nanosized Au particles in a Au/TiO(2) catalyst, J. Catal. 225 (2004) 86.
[16] T. Okazawa, M. Fujiwara, T. Nishimura, T. Akita, M. Kohyama, Y. Kido, Growth mode and electronic structure of Au nano-clusters on NiO(001) and TiO2(110), Surf. Sci. 600 (2006) 1331.
[17] T. Risse, S. Shaikhutdinov, N. Nilius, M. Sterrer, H.-J. Freund, Gold supported on thin oxide films: from single atoms to nanoparticles, Acc. Chem. Res. 41 (2008) 949.
[18] M. Zhou, A. Zhang, Z. Dai, Y.P. Feng, C. Zhang, Strain-enhanced stabilization and catalytic activity of metal nanoclusters on graphene, J. Phys. Chem. C 114 (2010) 16541.
[19] M. Chen, Y. Cai, Z. Yan, D.W. Goodman, On the origin of the unique properties of supported Au nanoparticles, J. Am. Chem. Soc. 128 (2006) 6341.
[20] D.C. Meier, D.W. Goodman, The influence of metal cluster size on adsorption energies: CO adsorbed on Au clusters supported on TiO2, J. Am. Chem. Soc. 126 (2004) 1892.
[21] K. Okazaki, S. Ichikawa, Y. Maeda, M. Haruta, M. Kohyama, Electronic structures of Au supported on TiO2, Appl. Catal. A Gen. 291 (2005) 45.
[22] M. Valden, X. Lai, D.W. Goodman, Onset of catalytic activity of gold clusters on titania with the appearance of nonmetallic properties, Science 281 (1998) 1647.
[23] C.H. Christensen, J.K. Norskov, A molecular view of heterogeneous catalysis, J. Chem. Phys. 128 (2008) 182503.
[24] T. Jiang, D.J. Mowbray, S. Dobrin, H. Falsig, B. Hvolbaek, T. Bligaard, J.K. Norskov, Trends in CO oxidation rates for metal nanoparticles and close-packed, stepped, and kinked surfaces, J. Phys. Chem. C 113 (2009) 10548.
[25] J.K. Norskov, T. Bligaard, B. Hvolbaek, F. Abild-Pedersen, I. Chorkendorff, C.H. Christensen, The nature of the active site in heterogeneous metal catalysis, Chem. Soc. Rev. 37 (2008) 2163.
[26] J.K. Norskov, T. Bligaard, J. Rossmeisl, C.H. Christensen, Towards the computational design of solid catalysts, Nat. Chem. 1 (2009) 37.
[27] V.R. Stamenkovic, B.S. Mun, M. Arenz, K.J.J. Mayrhofer, C.A. Lucas, G. Wang, P.N. Ross, N.M. Markovic, Trends in electrocatalysis on extended and nanoscale Pt-bimetallic alloy surfaces, Nat. Mater. 6 (2007) 241.
[28] T. Okazawa, M. Kohyama, Y. Kido, Electronic properties of Au nano-particles supported on stoichiometric and reduced TiO2 (110) substrates, Surf. Sci. 600 (2006) 4430.
[29] M.-F. Luo, C.-C. Wang, G.-R. Hu, W.-R. Lin, C.-Y. Ho, Y.-C. Lin, Y.-J. Hsu, Active alloying of Au with Pt in nanoclusters supported on a thin film of Al(2)O(3)/NiAl(100), J. Phys. Chem. C 113 (2009) 21054.
[30] H.G. Boyen, T. Herzog, G. Kastle, F. Weigl, P. Ziemann, J.P. Spatz, M. Moller, R. Wahrenberg, M.G. Garnier, P. Oelhafen, X-ray photoelectron spectroscopy study on gold nanoparticles supported on diamond, Phys. Rev. B 65 (2002).
[31] H.G. Boyen, G. Kastle, F. Weigl, P. Ziemann, G. Schmid, M.G. Garnier, P. Oelhafen, Chemically induced metal-to-insulator transition in Au55 clusters: effect of stabilizing ligands on the electronic properties of nanoparticles, Phys. Rev. Lett. 87 (2001) 276401.
[32] M. Buttner, P. Oelhafen, XPS study on the evaporation of gold submonolayers on carbon surfaces, Surf. Sci. 600 (2006) 1170.
[33] G.K. Wertheim, S.B. Dicenzo, S.E. Youngquist, Unit charge on supported gold clusters in photoemission final-state, Phys. Rev. Lett. 51 (1983) 2310.
[34] G.C. Bond, D.T. Thompson, Catalysis by gold, Catal. Rev. Sci. Eng. 41 (1999) 319.
[35] J.J. Yeh, I. Lindau, Atomic subshell photoionization cross-sections and asymmetry parameters — 1 less-than-or-equal-to z less-than-or-equal-to 103, At. Data Nucl. Data Tables 32 (1985) 1.
[36] P. Giannozzi, S. Baroni, N. Bonini, M. Calandra, R. Car, C. Cavazzoni, D. Ceresoli, G.L. Chiarotti, M. Cococcioni, I. Dabo, A. Dal Corso, S. de Gironcoli, S. Fabris, G. Fratesi, R. Gebauer, U. Gerstmann, C. Gougoussis, A. Kokalj, M. Lazzeri, L. Martin-Samos, N. Marzari, F. Mauri, R. Mazzarello, S. Paolini, A. Pasquarello, L. Paulatto, C. Sbraccia, S. Scandolo, G. Sclauzero, A.P. Seitsonen, A. Smogunov, P. Umari, R.M. Wentzcovitch, QUANTUM ESPRESSO: a modular and open-source software project for quantum simulations of materials, J. Phys. Condens. Matter 21 (2009).
[37] A. Dal Corso, A.M. Conte, Spin–orbit coupling with ultrasoft pseudopotentials: application to Au and Pt, Phys. Rev. B 71 (2005).
[38] D. Vanderbilt, Soft self-consistent pseudopotentials in a generalized eigenvalue formalism, Phys. Rev. B 41 (1990) 7892.
[39] R. Vanharde, F. Hartog, Statistics of surface atoms and surface sites on metal crystals, Surf. Sci. 15 (1969) (189-&).
[40] B.R. Cuenya, S.H. Baeck, T.F. Jaramillo, E.W. McFarland, Size- and support-dependent electronic and catalytic properties of Au-0/Au3+ nanoparticles synthesized from block copolymer micelles, J. Am. Chem. Soc. 125 (2003) 12928.
[41] M.G. Mason, Electronic-structure of supported small metal-clusters, Phys. Rev. B 27 (1983) 748.
[42] Y. Sohn, D. Pradhan, A. Radi, K.T. Leung, Interfacial electronic structure of gold nanoparticles on Si(100): alloying versus quantum size effects, Langmuir 25 (2009) 9557.
[43] Z.X. Yang, R.Q. Wu, Origin of positive core-level shifts in Au clusters on oxides, Phys. Rev. B 67 (2003).
[44] P.H. Citrin, G.K. Wertheim, Y. Baer, Core-level binding-energy and density of states from surface atoms of gold, Phys. Rev. Lett. 41 (1978) 1425.
[45] J. Radnik, C. Mohr, P. Claus, On the origin of binding energy shifts of core levels of supported gold nanoparticles and dependence of pretreatment and material synthesis, Phys. Chem. Chem. Phys. 5 (2003).
[46] M.P. Seah, G.C. Smith, M.T. Anthony, AES — energy calibration of electron spectrometers, 1. An absolute, traceable energy calibration and the provision of atomic reference line energies, Surf. Interface Anal. 15 (1990) 293.
[47] N. Weiher, E. Bus, L. Delannoy, C. Louis, D.E. Ramaker, J.T. Miller, J.A. van Bokhoven, Structure and oxidation state of gold on different supports under various CO oxidation conditions, J. Catal. 240 (2006) 100.

Please cite this article as: B.N. Reinecke, et al., Elucidating the electronic structure of supported gold nanoparticles and its relevance to catalysis by means of hard X-ray photoel..., Surf. Sci. (2016), http://dx.doi.org/10.1016/j.susc.2015.12.025

[48] H.G. Boyen, A. Ethirajan, G. Kastle, F. Weigl, P. Ziemann, G. Schmid, M.G. Garnier, M. Buttner, P. Oelhafen, Alloy formation of supported gold nanoparticles at their transition from clusters to solids: does size matter? Phys. Rev. Lett. 94 (2005).
[49] J.A. van Bokhoven, J.T. Miller, d electron density and reactivity of the d band as a function of particle size in supported gold catalysts, J. Phys. Chem. C 111 (2007) 9245.
[50] U. Gelius, L. Asplund, E. Basilier, S. Hedman, K. Helenelund, K. Siegbahn, A high-resolution multipurpose ESCA instrument with X-ray monochromator, Nucl. Instrum. Methods Phys. Res., Sect. B 229 (1984) 85.
[51] Z. Hussain, N.F.T. Hall, L.F. Wagner, S.P. Kowalczyk, C.S. Fadley, K.A. Thompson, R.L. Dod, Brillouin-zone averaging in angle-resolved X-ray photoemission from valence levels of single-crystal gold and aluminum, Solid State Commun. 25 (1978) 907.
[52] R. Meyer, C. Lemire, S.K. Shaikhutdinov, H. Freund, Surface chemistry of catalysis by gold, Gold Bull. 37 (2004) (72-+).
[53] P. Strasser, S. Koh, T. Anniyev, J. Greeley, K. More, C.F. Yu, Z.C. Liu, S. Kaya, D. Nordlund, H. Ogasawara, M.F. Toney, A. Nilsson, Lattice-strain control of the activity in dealloyed core-shell fuel cell catalysts, Nat. Chem. 2 (2010) 454.
[54] A. Balerna, E. Bernieri, P. Picozzi, A. Reale, S. Santucci, E. Burattini, S. Mobilio, A structural investigation on small gold clusters by EXAFS, Surf. Sci. 156 (1985) 206.
[55] A. Balerna, E. Bernieri, P. Picozzi, A. Reale, S. Santucci, E. Burattini, S. Mobilio, Extended X-ray-absorption fine-structure and near-edge-structure studies on evaporated small clusters of Au, Phys. Rev. B 31 (1985) 5058.
[56] J.T. Miller, A.J. Kropf, Y. Zha, J.R. Regalbuto, L. Delannoy, C. Louis, E. Bus, J.A. van Bokhoven, The effect of gold particle size on Au–Au bond length and reactivity toward oxygen in supported catalysts, J. Catal. 240 (2006) 222.
[57] W.J. Huang, R. Sun, J. Tao, L.D. Menard, R.G. Nuzzo, J.M. Zuo, Coordination-dependent surface atomic contraction in nanocrystals revealed by coherent diffraction, Nat. Mater. 7 (2008) 308.
[58] H. Falsig, B. Hvolbaek, I.S. Kristensen, T. Jiang, T. Bligaard, C.H. Christensen, J.K. Norskov, Trends in the catalytic CO oxidation activity of nanoparticles, Angew. Chem. Int. Ed. 47 (2008) 4835.
[59] V. Petkov, N. Bedford, M.R. Knecht, M.G. Weir, R.M. Crooks, W. Tang, G. Henkelman, A. Frenkel, Periodicity and atomic ordering in nanosized particles of crystals, J. Phys. Chem. C 112 (2008) 8907.
[60] T. Anniyev, H. Ogasawara, M.P. Ljungberg, K.T. Wikfeldt, J.B. MacNaughton, L.A. Naslund, U. Bergmann, S. Koh, P. Strasser, L.G.M. Pettersson, A. Nilsson, Complementarity between high-energy photoelectron and L-edge spectroscopy for probing the electronic structure of 5d transition metal catalysts, Phys. Chem. Chem. Phys. 12 (2010) 5694.

Please cite this article as: B.N. Reinecke, et al., Elucidating the electronic structure of supported gold nanoparticles and its relevance to catalysis by means of hard X-ray photoel..., Surf. Sci. (2016), http://dx.doi.org/10.1016/j.susc.2015.12.025